Invited Paper

Dual THz comb spectroscopy

Takeshi Yasui *
Tokushima University, Graduate School of Technology, Industrial and Social Sciences,
2-1 Minami-Josanjima, Tokushima, Tokushima 770-8506, Japan
* Email: yasui.takeshi@tokushima-u.ac.jp

（Received April 24 2018）

Abstract: Terahertz (THz) frequency combs are innovative tools for broadband THz spectroscopy because a series of comb modes can serve as frequency markers that are traceable to a frequency standard. However, usual THz spectrometer cannot resolve each mode of THz comb due to insufficient spectral resolution. Recently, dual THz comb spectroscopy appears as a new spectroscopic tool to acquire the mode-resolved THz comb spectrum with high resolution, high accuracy, broad spectral range, and moderate data acquisition time. In this paper, we have reviewed the recent progress of dual THz comb spectroscopy in our group.

Keywords: Terahertz spectroscopy, Frequency comb, Dual-comb spectroscopy, Gas spectroscopy

doi: 10.11906/TST.012-025.2019.03.02

1. Introduction

Recently, THz frequency combs have started to reveal their potential for THz frequency metrology [1, 2], such as spectroscopy [3-8], frequency measurement [9-16], and signal generation [17-19]. A THz comb, which is a description of THz pulse train in the frequency domain, is composed of a series of CW-THz waves regularly separated by a repetition frequency of THz pulse train. In the field of frequency metrology, a THz comb is attractive due to the narrow-linewidth of the CW-THz waves that provide regular frequency marks over a wide spectral band. Furthermore, the absolute frequencies of all comb modes can be phase-locked to a microwave or radio-frequency (RF) frequency standard by laser control. These characteristics enable us to use a THz comb as a precise ruler of THz frequency. For example, THz-comb-referenced frequency measurement has been successively applied to the measurement of absolute frequency in CW-THz sources with high accuracy and/or real time [9-16]. Also, THz comb was used for generation of the accurate THz frequency signal by phase-locking the CW-THz source to one mode of THz comb [17-19]. Furthermore, the THz comb can combine the merits of both THz time-domain spectroscopy (THz-TDS) and THz frequency-domain spectroscopy (THz-FDS) by the help of dual-comb spectroscopy [3, 20, 21], so that it can show the frequency scale of the spectrum based on a frequency standard.

In this paper, we have reviewed the recent progress of dual THz comb spectroscopy (THz-DCS). First, we have introduced the principle of operation in THz-DCS [5]. Second, a combination of the spectral interleaving technique with THz-DCS has been effectively applied to make the THz comb gapless [6]. Third, we have demonstrated the dynamic THz spectroscopy of molecular gas mixed with smoke [8].

2. THz-DCS

We first consider how we can acquire the mode-resolved spectrum of a THz comb, which surpasses spectral resolution of conventional THz spectrometer. A traditional THz-TDS system employing mechanical time-delay scanning usually measures the temporal waveform of a portion of a single THz pulse, as shown in Fig. 1(a). Taking the Fourier transformation (FT) of the waveform gives the continuous spectrum of the broadband THz radiation without comb structure, as shown in Fig. 1(b). On the other hand, if the time window is greatly expanded to cover more than one repetition period, one can measure the temporal waveform of consecutive THz pulses, i.e. a THz pulse train, as shown in Fig. 1(c). Taking the FT of this will give the mode-resolved spectrum of the THz comb because FT of the THz pulse train imprints a frequency modulation on THz spectrum, as shown in Fig. 1(d).

However, in conventional THz-TDS system it is not practical to measure such a temporal waveform of THz pulse train because it requires mechanical time-delay scanning over several meters. Instead, we focus on asynchronous-optical-sampling THz-TDS (ASOPS-THz-TDS) using two mode-locked lasers with slightly mismatched repetition frequencies [22]. Since ASOPS-THz-TDS enables us to expand ps time scale of THz pulse up to the μs scale, the resulting slow-downed temporal waveform can be directly measured by a standard oscilloscope or digitizer without the need for the mechanical time-delay scanning. One can therefore arbitrarily adjust the observed time window of THz pulse temporal waveform by changing the time scale of the oscilloscope. Therefore, it is possible to extend the time window to more than one repetition period due to its non-mechanical nature of the time-delay scanning.

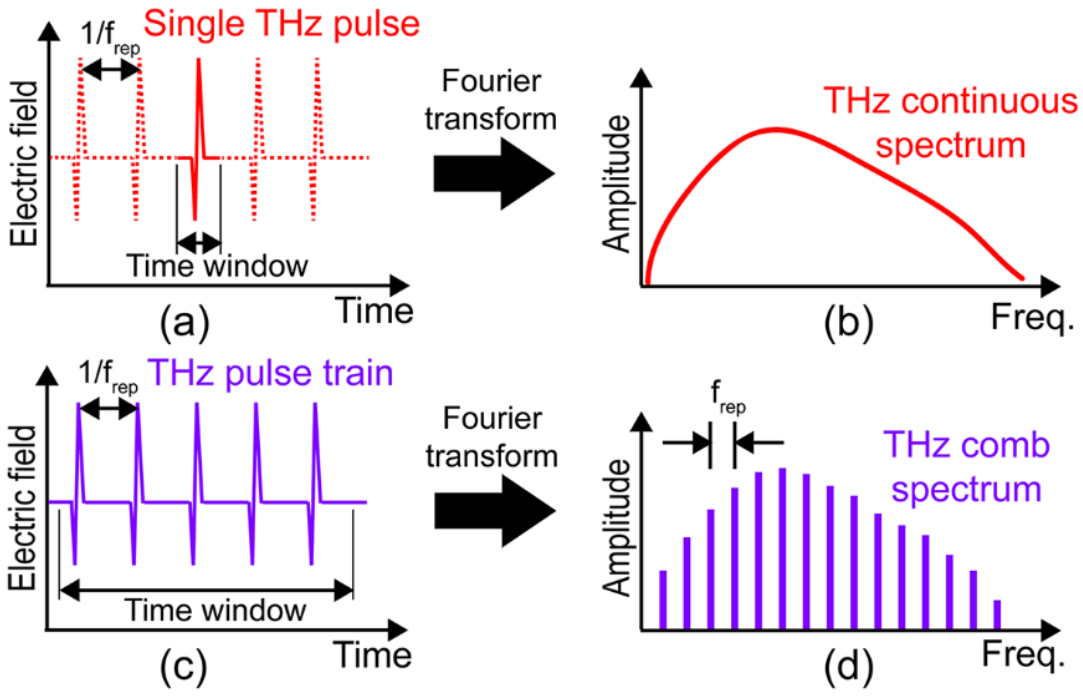

Fig. 1 (a) Temporal waveform of single THz pulse and (b) corresponding THz continuous spectrum. (c) Temporal waveform of THz pulse train and (d) corresponding THz comb spectrum.

THz-DCS system consists of dual mode-locked Er-fiber lasers (center wavelength = 1550 *nm*, pulse duration = 50 *fs*, mean power = 500 *mW*, f_{rep1} = 250,000,000 *Hz*, f_{rep2} = 250,000,050 *Hz*, $\Delta f_{rep} = f_{rep2} - f_{rep1}$ = 50 *Hz*) and a delay-stage-free THz-TDS setup including a pair of photoconductive antennae (PCA) as shown in Fig. 2. f_{rep1} and f_{rep2} were stabilized by two independent laser control systems referenced to a rubidium frequency standard (Rb-FS). After wavelength conversion of the two laser beams by second-harmonic-generation crystals (SHGs), THz pulse train was emitted by a dipole-shaped, low-temperature-grown, GaAs PCA (LT-GaAs-PCA) triggered by pump light (PCA1; pump power = 18 *mW*, bias voltage = 20 *V*), and was then detected by another dipole-shaped LT-GaAs-PCA triggered by probe light (PCA2; probe power = 9 *mW*). Portions of the output light from the two lasers were fed into a sum-frequency-generation cross-correlator (SFG-XC). The resulting SFG signal was used to generate a time origin signal in the ASOPS-THz-TDS. After amplification with a current preamplifier (AMP), the temporal waveform of the output signal from PCA2 was acquired with a digitizer (sampling rate = 2*MS/s*, resolution = 20 *bit*) by using the SFG-XC signal as a trigger signal. Then, time scale of the observed signal was calibrated by a temporal magnification factor of $f_{rep1}/\Delta f_{rep}$ (= 250,000,000/50 = 5,000,000). Finally, the amplitude spectrum of THz comb was obtained by FT of the temporal waveform of THz pulse train.

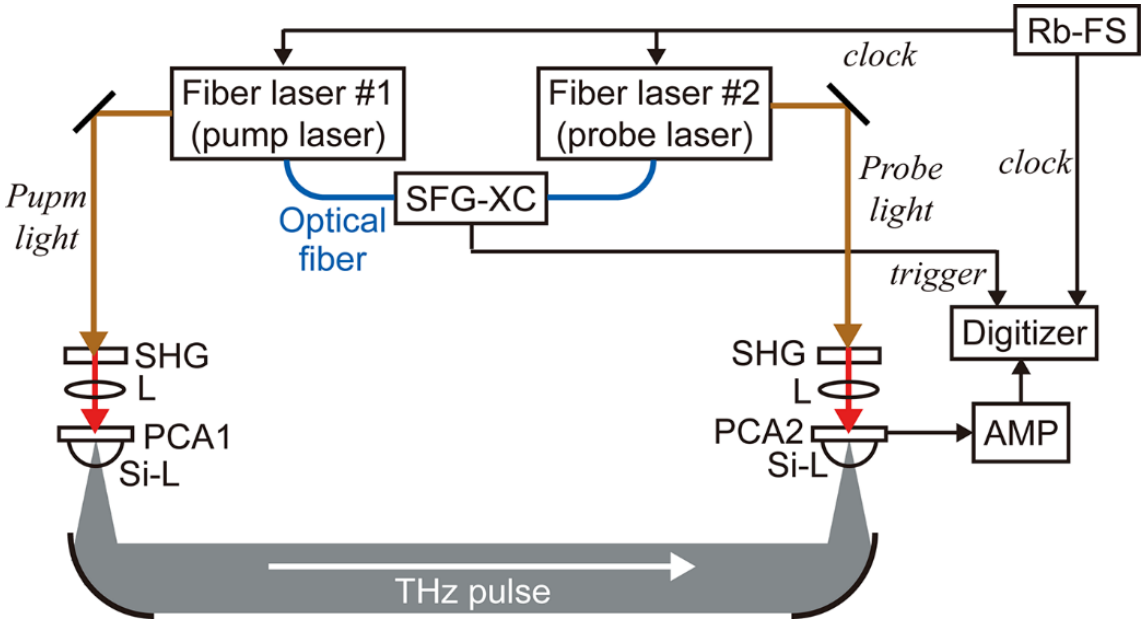

Fig. 2 Experimental setup. Rb-FS, rubidium frequency standard; SFG-XC, sum-frequency-generation cross-correlator; SHGs, second-harmonic-generation crystals; Ls, lenses; EDFA, erbium-doped fiber amplifier; OSC, erbium-doped fiber oscillator; PCA1, dipole-shaped LT-GaAs photoconductive antenna for THz generation; PCA2, dipole-shaped LT-GaAs photoconductive antenna for THz detector; Si-Ls, silicon lenses; AMP, current preamplifier.

Figure 3(a) shows the acquired temporal waveform of the THz pulse train. 10 consecutive THz pulses are clearly observed at an interval of 4 *ns*. Figure 3(b) shows a magnified temporal waveform of the first THz pulse. The transient evolution of the pulsed THz radiation in the picosecond region was also observed clearly. The black line in Fig. 3(c) shows the amplitude spectrum of the THz comb obtained by taking the FT of the THz pulse train in Fig. 3(a). For comparison, the gray line in Fig. 3(c) shows a continuous spectrum of the THz amplitude obtained by taking the FT of a single THz pulse (time window = 4 *ns*) measured with one-pulse-period ASOPS-THz-TDS. The spectral envelop of the THz comb spectrum is in good agreement with the spectral shape of the THz continuous spectrum. This indicates that our THz-DCS can capture the temporal waveform of THz pulse train correctly. The spectrum of THz comb is composed of a series of frequency spikes regularly separated by the repetition frequency of the laser. To observe its detailed structure, we expanded the spectral region around 0.5570 *THz*, as shown in Fig. 3(d). The THz comb modes have a frequency spacing of 250 *MHz* and a linewidth of 25 *MHz*. The frequency spacing was equal to the mode-locked frequency of the fiber laser, whereas the linewidth was consistent with the reciprocal of the temporal window in Fig. 3(a) (= 40 *ns*).

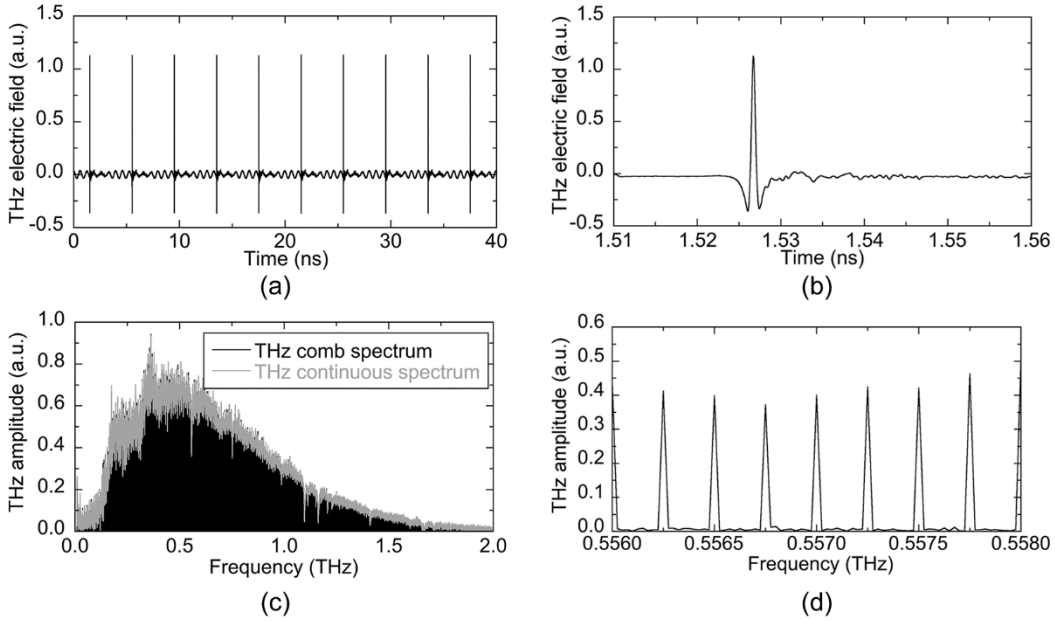

Fig. 3 Temporal waveform of electric field in (a) 10 consecutive THz pulses (time window = 40 ns) and (b) the first THz pulse (time window = 50 *ps*). (c) Comparison of amplitude spectrum between THz comb spectrum and THz continuous spectrum. (d) Amplitude spectrum of THz comb mode around 0.557 *THz*.

3. Gap-less THz-DCS

THz-DCS enables us to achieve a frequency resolution equal to the comb mode linewidth (typically, less than 1 *MHz*). However, the spectral sampling interval is limited to the comb mode spacing (typically, from several tens to a few hundred MHz) due to the excessively discrete mode distribution. If the comb mode gap is filled by interleaving additional frequency marks, the spectral sampling density and accuracy would be vastly enhanced in the broadband spectroscopy. The combination of such interleaving with dual-comb spectroscopy makes it possible to reduce the spectral sampling interval down to the comb mode linewidth.

Let us consider how we could interleave the additional marks into the gap produced between the comb modes of a THz comb. The THz comb is a harmonic frequency comb of the laser repetition frequency f_{rep1}. Therefore, the absolute frequency of each comb mode (= mf_{rep1}, where m is the order of THz comb modes) can be tuned by changing f_{rep1}. For example, since a single sweep of f_{rep1} by δf_{rep1} causes a frequency shift of m-order mode (freq. = mf_{rep1}) by $m\delta f_{rep1}$, M-times repetition of this sweep will lead to a total shift of $Mm\delta f_{rep1}$ in mf_{rep1}. If incremental sweeping of the comb mode is repeated at an interval equal to the mode linewidth, and all of the resulting comb spectra are overlaid in the spectral domain, as shown in Fig. 4, the frequency gaps of a THz comb can be completely removed. To fill the frequency gaps, such incremental sweeping has to be repeated times of M. In this way, a spectrally interleaved or gap-less THz comb will be achieved. This is

equivalent to continuous sweeping of a single-mode, narrow-linewidth CW-THz wave. The resulting spectral sampling interval will be equal to the linewidth of the comb mode. It is important to note that M is sufficiently large to fully interleave the comb gap because the tunable range of f_{rep1} is within 1 % of f_{rep1} at maximum.

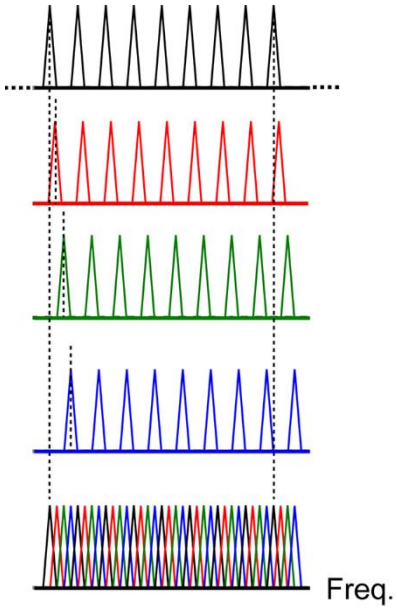

Fig. 4 Spectrally interleaved THz comb achieved by incremental sweeping of THz comb mode and spectral overlapping.

To demonstrate the effectiveness of the gap-less THz comb, we first performed the gap-less THz-DCS of water vapor. Here, the rotational transition $1_{10} \leftarrow 1_{01}$ at 0.557 *THz* in water vapor was measured. A sample gas, a mixture of water vapor (partial pressure = 10 *Pa*) and nitrogen (partial pressure = 320 *Pa*), was introduced into the low-pressure gas cell. The sample has an expected pressure-broadening linewidth of 23 *MHz* full-width at half-maximum (FWHM) from the self-broadening of water vapor and the collision-broadening induced by nitrogen and an expected Doppler-broadening linewidth of 0.026 *MHz*. The experimental setup used here is shown in Fig. 2. Figure 5(a) shows the amplitude spectrum of the THz comb expanded around 0.557 *THz* before spectral interleaving. The comb modes had a frequency gap of 250 *MHz* and a linewidth of 25 *MHz*. This mode gap was exactly equal to f_{rep1}. On the other hand, the mode linewidth here was determined by the reciprocal of the temporal window (= 40 *ns*). The amplitude spectrum without incremental sweeping of the THz comb modes did not indicate the spectral shape of the absorption line due to the excessively coarse distribution of the comb modes compared with the absorption linewidth of the low-pressure water vapor.

Next, we demonstrated incremental sweeping of the comb modes across the absorption line at 0.557 *THz* by changing the repetition frequencies of both lasers. Incremental increases of f_{rep1} and f_{rep2} (= $f_{rep1} + \Delta f_{rep}$) by 11,220.8 *Hz* (= $\delta f_{rep1} = \delta f_{rep2}$) were repeated 10 *times* while keeping Δf_{rep} at 50 *Hz*. The resulting overlaid spectra of the comb modes are shown in Fig. 5(b). In this

demonstration, a single shift of Δf_{rep} by 0.004488 % resulted in sweeping of the comb modes by 10 % of their interval (= 25 *MHz*) due to the large number of THz comb modes (m = 2,228 at 0.557 *THz*). The frequency gaps between the comb modes in Fig. 5(a) were filled by interleaving additional frequency marks. In other words, a spectrally interleaved THz comb was successfully achieved. Although the comb mode amplitude is undulated due to a slight mismatching between the comb mode peaks and the spectral sampling points, a sharp spectral dip clearly appeared at the position of the water absorption line of $1_{10} \leftarrow 1_{01}$. The absorption was extracted from the power spectrum by taking the peak amplitude of each mode normalized with a reference spectrum obtained under identical conditions (not shown). To determine the spectral linewidth, we fitted a Lorentzian function to the measured spectral profile because the spectral shape in THz region arises from the pressure broadening rather than Doppler broadening (= 0.026 *MHz*) at the present experimental condition. As a result, the spectral linewidth was determined to be 24 *MHz*, and this value is consistent with the expected pressure broadening linewidth (= 23 *MHz*).

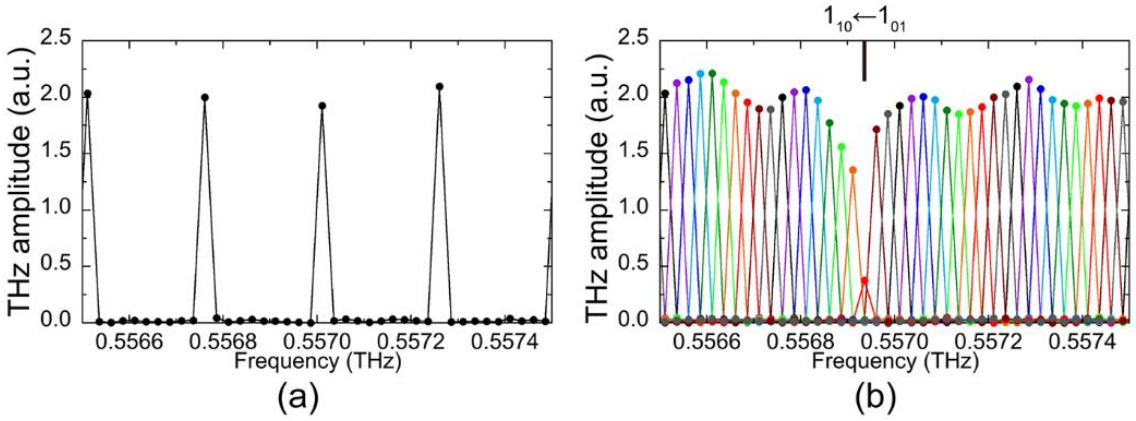

Fig. 5 Amplitude spectra of (a) standard THz comb and (c) interleaved THz comb around 0.557 *THz* after passing through low-pressure water vapor contained in the gas cell.

We next performed gas-phase spectroscopy of CH_3CN because this molecule is a very abundant species in the interstellar medium and is an ideal observational probe of the kinetic temperature and density of interstellar clouds. Since CH_3CN is a symmetric top molecule with a rotational constant B of 9.2 *GHz*, it displays two features: a series of manifolds of rotational transitions regularly spaced by *2B* (= 18.4 *GHz*), and hyperfine structure of rotational transitions into each manifold determined by the centrifugal distortion constant D_{JK}. The reduced comb-mode linewidth and increased spectral sampling density offered by the gap-less THz-DCS should allow the hyperfine structure to be resolved at high resolution and accuracy. Figure 6(a) shows the absorption spectrum of this gas sample obtained by using the usual THz comb, in which a series of manifolds from J = 16 to J = 55 was clearly confirmed at intervals of 18.4 *GHz* within a frequency range from 0.3 to 1.0 *THz*. Next, we used an interleaved THz comb with a mode linewidth of 25 *MHz* for high-precision spectroscopy and allowed the hyperfine structure into a single manifold around 0.64 *THz* (J = 35 to J = 34) to be observed, as shown in Fig. 6(b). To assign these absorption lines, multi-

peak fitting analysis based on a Lorentzian function was used, indicated by the red solid line in Fig. 6(b). In comparison with literature values reported in the JPL database (see blue dashed line), we successfully assigned lines K = 2 to 10 within a frequency discrepancy of 4.7 ± 2.6 *MHz* (mean ± standard deviation for 9 absorption lines). To assign lines K = 0 and 1 with the frequency separation of 12 *MHz*, the linewidth and incremental step of the comb modes should be further reduced. To this end, we expanded the time window to 400 *ns*, in which the temporal waveform of 100 consecutive THz pulses was measured. Figure 6(c) indicates that two spectral dips clearly appear although the pressure broadening makes them overlap partially. The spectral linewidth is determined to be 7.5 *MHz* for K = 0 and 6.1 *MHz* for K = 1 by performing multi-peak fitting analysis, which are consistent with the expected pressure broadening linewidth (= 5.9 *MHz*). These results clearly indicated that the reduced comb-mode linewidth and the increased spectral sampling density further enhanced the spectral resolution. We also determined their center frequencies to be 0.643257578 *THz* for K = 0 and 0.643269502 *THz* for K = 1 from the multi-peak fitting analysis. The discrepancy of the center frequencies from the literature values in the JPL database (see blue dashed line) was 0.578 *MHz* for K = 0 and 0.502 *MHz* for K = 1, corresponding to a mean spectral accuracy of 8.39×10^{-7}. These results clearly indicated the high potential of the spectrally interleaved dual-THz-comb spectroscopy to simultaneously probe multiple absorption lines of low-pressure molecular gas.

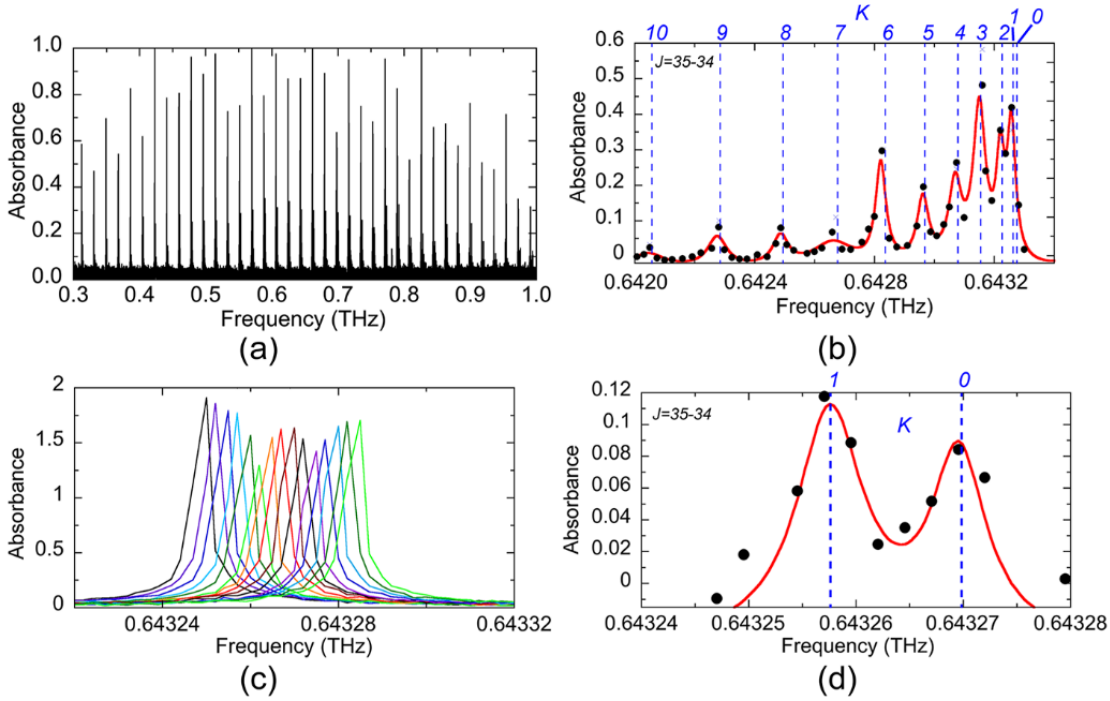

Fig. 6 Absorption spectrum of low-pressure acetonitrile gas (a) within a frequency range from 0.3 to 1 *THz* and (b) around 0.6428 *THz*. (c) Amplitude spectrum and (d) absorption spectrum obtained 15 incremental sweeps of THz comb mode across two adjacent absorption peaks.

4. Dynamic THz spectroscopy of molecular gas mixed with smoke

THz region is a characteristic frequency band in which many absorption lines due to rotational transitions of polar gas molecules appear. Instead of the intermolecular vibration spectrum observed in the infrared region, if the molecular rotational transition spectrum observed in the THz region could be used, high selectivity and high sensitivity would be expected. In addition, from the relationship between the wavelength of THz radiation and the size of minute particles, there is less susceptibility to optical scattering by aerosols. Therefore, under conditions in which aerosols are mixed with the gas to be analyzed, as in the combustion processes or the fire accident, THz spectroscopy is considered as a useful technique for simultaneously analyzing the target gas molecule species in a straightforward and rapid manner. To demonstrate the potential of THz-DCS for real-time monitoring of gas molecules mixed with unwanted aerosols, we applied our THz-DCS system to the dynamic THz spectroscopy of acetonitrile (CH_3CN) gas, which is a target gas, in the presence of smoke, which is an unnecessary aerosol, at the atmospheric pressure.

Figure 7 shows a schematic diagram of the experimental setup, which contains dual repetition-frequency-stabilized, mode-locked Er-fiber lasers (center wavelength = 1550 *nm*, pulse duration = 50 *fs*, f_{rep1} = 250,000,000 *Hz*, f_{rep2} = 250,000,050 *Hz*, $\Delta f_{rep} = f_{rep2} - f_{rep1}$ = 50 *Hz*), a pair of fiber-coupled LT-InGaAs/InAlAs PCAs, and a THz optical setup including a gas cell. The pulsed THz radiation was emitted from a strip-line-shaped LT-InGaAs/InAlAs PCA emitter (PCA1) triggered by pump light, passed through the gas cell after being collimated with a THz lens, and was then focused onto a dipole-shaped LT-InGaAs/InAlAs PCA detector (PCA2) triggered by probe light. The temporal waveform of the pulsed THz electric field was obtained at 50 *Hz* with a sampling interval of 100 *fs* by acquiring the current signal from PCA2 with a digitizer. After accumulating 50 temporal waveforms, we selected the first quarter of its whole temporal waveform in the pulsed THz electric field (pulse period = 4 *ns*), corresponding to a time delay from 0 to 1 *ns*, to obtain a THz amplitude spectrum by Fourier transform. Finally, a THz power spectrum with a frequency resolution of 1 *GHz* was acquired at a scan rate of 1 *Hz* for dynamic THZ spectroscopy of the sample gas.

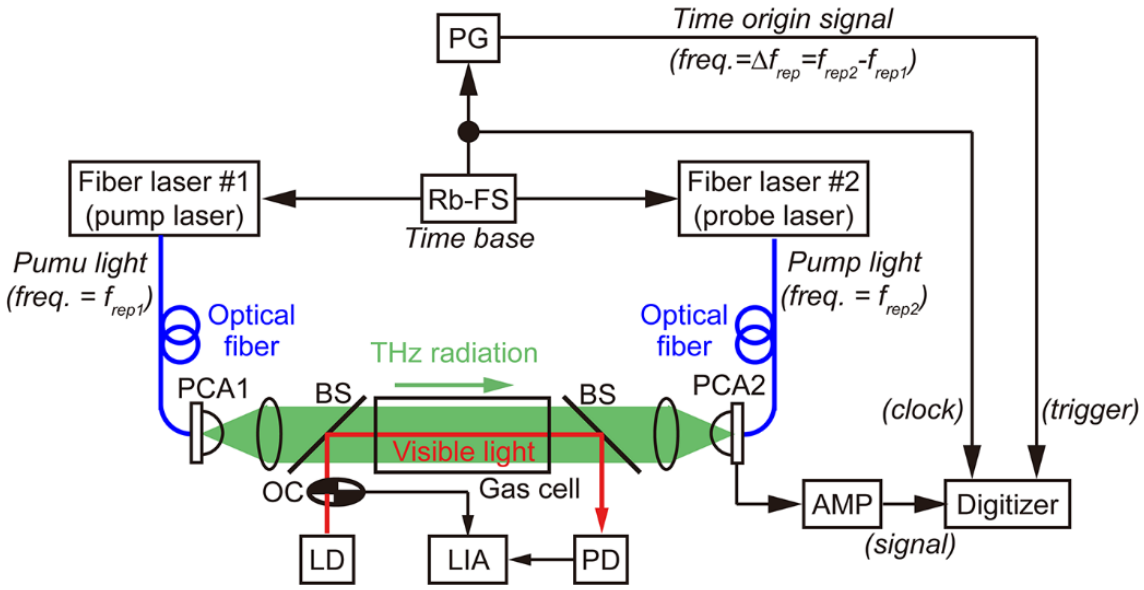

Fig. 7 Experimental setup. Rb-FS: rubidium frequency standard; PCA1: strip-line-shaped LT-InGaAs/InAlAs photoconductive antenna for THz generation; BSs: pellicle beam-splitters; PCA2: dipole-shaped LT-InGaAs/InAlAs photoconductive antenna for THz detection; AMP: current preamplifier; LD: laser diode (λ = 635 *nm*); OC: optical chopper; PD: photodetector; LIA: lock-in amplifier; PG: pulse generator.

To experimentally confirm the robustness of THz radiation to scattering by the aerosols, we measured the signal attenuation of broadband THz radiation and visible light in the presence of smoke from the incense stick. The THz radiation and visible light from a laser diode (LD; wavelength = 635 *nm*, average power = 3 *mW*) were made to collinearly overlap with a pellicle beam-splitter (BS) and then co-propagated in the gas cell (length = 200 *mm*, diameter = 50 *mm*). After passing through the cell, the visible light was separated again by another BS and was measured using a combination of an optical chopper (OC), a photodetector (PD), and a lock-in amplifier (LIA). The THz power spectrum and the visible light intensity were measured at intervals of 1 *s* during a 50 *s* period. The incense stick was burned for 20 *s* after the start of the measurement in the gas cell A. Red and green plots in Fig. 8(a) show the temporal change of the THz power at 0.6 *THz* and the visible light intensity before and after burning the incense stick. Although the scattering by the smoke reduced the visible light intensity by about 1/175, the THz power was almost constant before and after burning the incense stick. THz power values were $(3.97 \pm 1.44) \times 10^{-9}$ before burning and $(3.44 \pm 0.76) \times 10^{-9}$ after burning. THz power spectra of the signal and noise before and after burning the incense stick are shown in Figs. 8(b) and 8(c). Although sharp absorption lines always appeared at 0.557 *THz* and 0.752 *THz* due to the atmospheric water vapor inside and outside of the cell, the spectral shape was not distorted at all during the measurement, indicating no scattering or absorption by the smoke. In this way, we confirmed the high robustness of THz radiation to the smoke from the viewpoint of both the THz power value and the spectral shape.

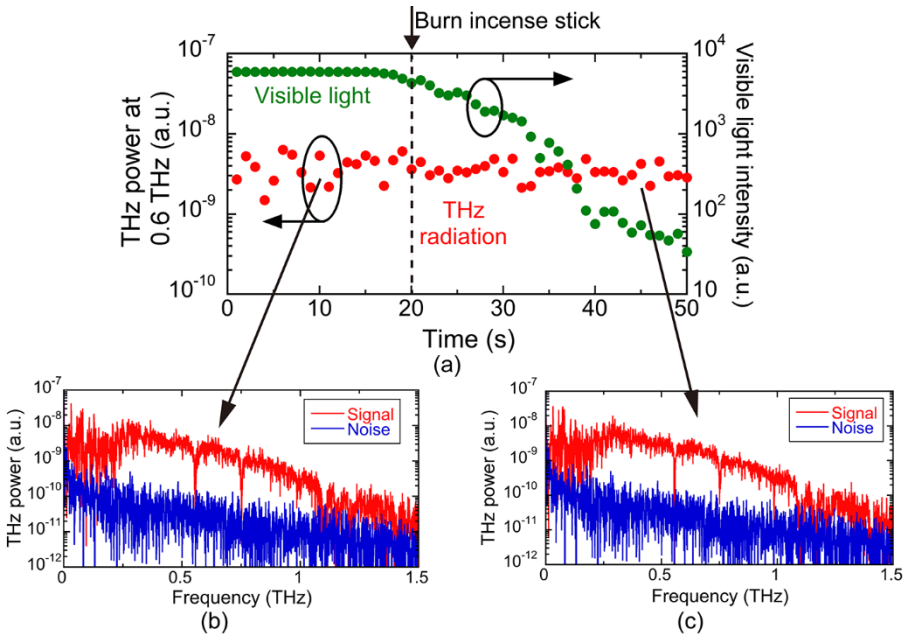

Fig. 8 (a) Temporal change of THz power at 0.6 *THz* (red plot, left vertical axis) and visible light intensity at 635 *nm* (green plot, right vertical axis) before and after injection of smoke by burning an incense stick. THz power spectra (b) before (= 10 *s*) and (c) after (= 45 *s*) burning the incense stick.

Finally, we performed dynamic THz spectroscopy of CH_3CN gas mixed with smoke in the gas cell at the atmospheric pressure. The enclosed gas cell was filled with smoke beforehand by placing the burning incense stick into the gas cell via the side window. A few droplets of CH_3CN liquid were dripped in the gas cell from its side window after opening it for a while, and then the window was closed again. The change in the CH_3CN gas concentration, associated with volatilization of CH_3CN droplets and the following diffusion of the volatilized CH_3CN gas, was monitored under smoky conditions by dynamic THz spectroscopy. After putting the CH_3CN droplets in the gas cell, we recorded the power spectrum of the broad THz radiation with a spectral resolution of 1 *GHz* every 1*s* for 50 *s*.

Figure 9(a) shows the temporal change of the THz power spectrum with respect to elapsed time. Immediately after the start of measurement, only the absorption lines of atmospheric water vapor are visible in the power spectrum. During the first 10 seconds, no absorption lines of CH_3CN gas can be clearly identified because the gas concentration was below the lower detection limit in the present system. The absorption lines of CH_3CN can be observed at 15 *s* and can be easily distinguished after 30 *s*. In this way, we succeeded in monitoring the temporal change of absorption lines superimposed on the broad THz spectrum in real time. By the curve fitting analysis with multiple Lorentzian functions, the molecular fraction of CH_3CN and water vapor was determined as a function of time and shown in Fig. 9(b). As the evaporation of the liquid CH3CN increases we observed a slight reduction in the water concentration due to its displacement. The CH_3CN concentration determined at t = 100 *s* is probably underestimated due to the saturation of the

spectrometer. The uncertainty of CH_3CN concentration is 200 *ppm* that can be considered as the detection limit of the present system for a measurement time of 1 *s*. An identical procedure for water vapor gave an estimated detection limit of 0.1 %.

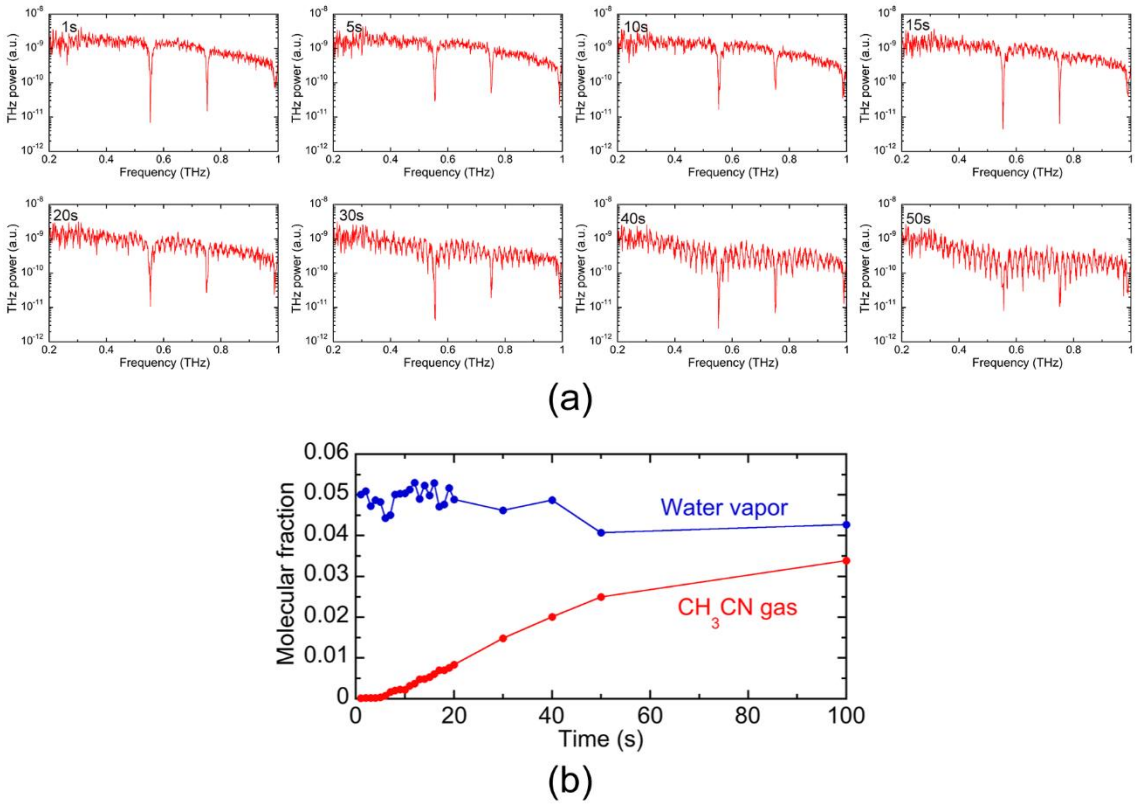

Fig. 9 (a) Temporal change of THz power spectra during volatilization of CH_3CN droplets and diffusion of CH_3CN in the gas cell filled with smoke. (b) Temporal change of the molecular fraction in CH_3CN and water vapor when CH_3CN droplets were volatilized and the volatilized CH_3CN gas was diffused in the gas cell filled with the smoke.

5. Summary

In this paper, we have reviewed the recent progress of THz-DCS in our group. THz-DCS can combine both advantage of THz-TDS and THz-FDS (namely, broad spectral range and high spectral resolution) while securing the frequency traceability to a microwave or RF frequency standard via TH comb. Simultaneous achievement of high resolution, high accuracy, broad spectral coverage, and moderate data acquisition time will be a powerful tool for THz spectroscopic applications.

Acknowledgements

This work was supported by grants for the Exploratory Research for Advanced Technology (ERATO) MINOSHIMA Intelligent Optical Synthesizer (IOS) Project (JPMJER1304) from the Japanese Science and Technology Agency.

References

[1] T. Yasui, S. Yokoyama, H. Inaba, et al.. "Terahertz frequency metrology based on frequency comb". *IEEE J. Selected Topics in Quantum Electron.*, 17, 191-201 (2011).

[2] H. Füser and M. Bieler. "Terahertz frequency combs". *J. Infrared Millim. Terahertz Waves*, 35, 585–609 (2014).

[3] T. Yasui, Y. Kabetani, E. Saneyoshi, et al.. "Terahertz frequency comb by multi-frequency-heterodyning photoconductive detection for high-accuracy, high-resolution terahertz spectroscopy". *Appl. Phys. Lett.*, 88, 241104 (2006).

[4] T. Yasui, M. Nose, A. Ihara, et al.. "Fiber-based, hybrid terahertz spectrometer using dual fiber combs". *Opt. Lett.*, 35, 1689-1691 (2010).

[5] Y.-D. Hsieh, Y. Iyonaga, Y. Sakaguchi, et al.. "Terahertz comb spectroscopy traceable to microwave frequency standard". *IEEE Trans. Terahertz Sci. Tech.*, 3 , 322-330 (2013).

[6] Y.-D. Hsieh,Y. Iyonaga,Y. Sakaguchi, et al.. "Spectrally interleaved, comb-mode-resolved spectroscopy using swept dual terahertz combs". *Sci. Rep.*, 4, 3816 (2014).

[7] T. Yasui, R. Ichikawa, Y.-D. Hsieh, et al.. "Adaptive sampling dual terahertz comb spectroscopy using dual free-running femtosecond lasers". *Sci. Rep.*, 5, 10786 (2015).

[8] Y.-D. Hsieh, S. Nakamura, D. G. Abdelsalam, et al.. "Dynamic terahertz spectroscopy of gas molecules mixed with unwanted aerosol under atmospheric pressure using fibre-based asynchronous-optical-sampling terahertz time-domain spectroscopy". *Sci. Rep.*, 6, 28114 (2016).

[9] S. Yokoyama, R. Nakamura, M. Nose, et al.. "Terahertz spectrum analyzer based on a terahertz frequency comb". *Opt. Express*, 16, 13052-13061 (2008).

[10] T. Yasui, R. Nakamura, K. Kawamoto, et al.. "Real-time monitoring of continuous-wave terahertz radiation using a fiber-based, terahertz-comb-referenced spectrum analyzer". *Opt. Express*, 17, 17034-17043 (2009).

[11] D.-S. Yee, Y. Jang, Y. Kim, et al.. "Terahertz spectrum analyzer based on frequency and power measurement". *Opt. Lett.*, 35, 2532-2534 (2010).

[12] H. Füser, R. Judaschke, and M. Bieler. "High-precision frequency measurements in the THz spectral region using an unstabilized femtosecond laser". *Appl. Phys. Lett.*, 99, 121111 (2011).

[13] H. Ito, S. Nagano, M. Kumagai, et al.. "Terahertz frequency counter with a fractional frequency uncertainty at the 10^{-17} level". *Appl. Phys. Express*, 6, 102202 (2013).

[14] T. Yasui, K. Hayashi, R. Ichikawa, et al.. "Real-time absolute frequency measurement of continuous-wave terahertz radiation based on dual terahertz combs of photocarriers with different frequency spacings". *Opt. Express*, 23, 11367-11377 (2015).

[15] T. Minamikawa, K. Hayashi, T. Mizuguchi, et al.. "Real-time determination of absolute frequency in continuous-wave terahertz radiation with a photocarrier terahertz frequency comb induced by an unstabilized femtosecond laser". *J. Infrared Millim. Terahertz Waves*, 37, 473-485 (2016).

[16] G. Hu, T. Mizuguchi, X. Zhao, et al.. "Measurement of absolute frequency of continuous-wave terahertz radiation in real time using a free-running, dual-wavelength mode-locked, erbium-doped fibre laser". *Sci. Rep.*, 7, 42082 (2017).

[17] M. Y. Tretyakov, A. P. Shkaev, A. M. Kiselev, et al.. "Frequency stabilization of a primary subterahertz oscillator by a frequency comb of a femtosecond laser". *JETP Lett.*, 91, 222-225 (2010).

[18] S. Barbieri , P. Gellie , G. Santarelli , et al.. "Phase-locking of a 2.7-THz quantum cascade laser to a mode-locked erbium-doped fibre laser". *Nat. Photon.*, 4, 636–640 (2010).

[19] M. Ravaro, C. Manquest, C. Sirtori, et al.. "Phase-locking of a 2.5 THz quantum cascade laser to a frequency comb using a GaAs photomixer". *Opt. Lett.*, 36, 3969-3971 (2011).

[20] S. Schiller. "Spectrometry with frequency combs". *Opt. Lett.*, 27, 766–768 (2002).

[21] F. Keilmann, C. Gohle, and R. Holzwarth. "Time-domain mid-infrared frequency-comb spectrometer". *Opt. Lett.*, 29, 1542–1544 (2004).

[22] T. Yasui, E. Saneyoshi and T. Araki. "Asynchronous optical sampling terahertz time-domain spectroscopy for ultrahigh spectral resolution and rapid data acquisition". *Appl. Phys. Lett.*, 87, 061101 (2005).

* URL: http://femto.me.tokushima-u.ac.jp/eng/